Engineering of near-IR photon pairs to be factorable in space-time and entangled in polarization

Kevin Zielnicki,[1,*] **Karina Garay-Palmett,**[2] **Radhika Dirks,**[3] **Alfred B. U'Ren,**[4] **and Paul G. Kwiat** [1]

[1]*Department of Physics, University of Illinois at Urbana-Champaign, Urbana, IL 61801, USA*
[2]*Departamento de Óptica, Centro de Investigación Científica y de Educación Superior de Ensenada, Apartado Postal 360 Ensenada, BC 22860, Mexico*
[3]*Seldn, Palo Alto, CA 94301, USA*
[4]*Instituto de Ciencias Nucleares, Universidad Nacional Autónoma de México, apdo. postal 70-543, 04510 D.F., Mexico*
[*]*kzielni2@illinois.edu*

Abstract: We present a source of near-infrared photon pairs based on the process of spontaneous parametric downconversion (SPDC), for which the joint signal-idler quantum state is designed to be factorable in the frequency-time and in the transverse position-momentum degrees of freedom. Our technique is based on the use of a broadband pump and vector group velocity matching between the pump, signal, and idler waves. We show experimentally that a source based on this technique can be configured for the generation of: i) pure heralded single photons, and ii) polarization-entangled photon pairs which are free from spectral correlations, in both cases without resorting to spectral filtering. While critical for many applications in optical quantum information processing, such a source has not previously been demonstrated.

OCIS codes: (190.4410) Nonlinear optics, parametric process; (270.5585) Quantum information and processing.

References and links

1. P. G. Kwiat, P. H. Eberhard, A. M. Steinberg, and R. Y. Chiao, "Proposal for a loophole-free bell inequality experiment," Phys. Rev. A **49**, 3209–3220 (1994).
2. N. Brunner, D. Cavalcanti, S. Pironio, V. Scarani, and S. Wehner, "Bell nonlocality," Rev. Mod. Phys. **86**, 419–478 (2014).
3. A. Barenco, D. Deutsch, A. Ekert, and R. Jozsa, "Conditional quantum dynamics and logic gates," Phys. Rev. Lett. **74**, 4083–4086 (1995).
4. E. Knill, R. Laflamme, and G. J. Milburn, "A scheme for efficient quantum computation with linear optics," Nature **409**, 46–52 (2001).
5. J. L. O'Brien, "Optical quantum computing," Science **318**, 1567–1570 (2007).
6. C. H. Bennett, G. Brassard, C. Crépeau, R. Jozsa, A. Peres, and W. K. Wootters, "Teleporting an unknown quantum state via dual classical and einstein-podolsky-rosen channels," Phys. Rev. Lett. **70**, 1895–1899 (1993).
7. D. Bouwmeester, J. W. Pan, K. Mattle, M. Eibl, H. Weinfurter, and A. Zeilinger, "Experimental quantum teleportation," Nature **390**, 575–579 (1997).
8. C. H. Bennett and G. Brassard, "Quantum cryptography: Public key distribution and coin tossing," in "Proceedings of IEEE International Conference on Computers, Systems and Signal Processing," vol. 1 (1984), pp. 175–179.
9. A. K. Ekert, "Quantum cryptography based on bell's theorem," Phys. Rev. Lett. **67**, 661–663 (1991).

#228272 - $15.00 USD Received 2 Jan 2015; revised 10 Mar 2015; accepted 10 Mar 2015; published 18 Mar 2015

10. C. Hong and L. Mandel, "Experimental realization of a localized one-photon state," Phys. Rev. Lett. **56**, 58–60 (1986).
11. K. T. McCusker and P. G. Kwiat, "Efficient optical quantum state engineering," Phys. Rev. Lett. **103**, 163602 (2009).
12. B. L. Glebov, J. Fan, and A. Migdall, "Deterministic generation of single photons via multiplexing repetitive parametric downconversions," Appl. Phys. Lett. **103**, 031115 (2013).
13. P. Kwiat, A. Steinberg, R. Chiao, P. Eberhard, and M. Petroff, "High-efficiency single-photon detectors," Phys. Rev. A **48**, R867–R870 (1993).
14. J. Brendel, N. Gisin, W. Tittel, and H. Zbinden, "Pulsed energy-time entangled twin-photon source for quantum communication," Phys. Rev. Lett. **82**, 2594 (1999).
15. A. Mair, A. Vaziri, G. Weihs, and A. Zeilinger, "Entanglement of the orbital angular momentum states of photons," Nature **412**, 313–316 (2001).
16. W. P. Grice, A. B. U'ren, and I. A. Walmsley, "Eliminating frequency and space-time correlations in multiphoton states," Phys. Rev. A **64**, 63815 (2001).
17. A. B. U'Ren, K. Banaszek, and I. A. Walmsley, "Photon engineering for quantum information processing," Quantum Inform. Compu. **3**, 480–502 (2003).
18. A. B. U'Ren, C. Silberhorn, J. L. Ball, K. Banaszek, and I. A. Walmsley, "Characterization of the nonclassical nature of conditionally prepared single photons," Phys. Rev. A **72**, 021802 (2005).
19. A. F. Abouraddy, M. B. Nasr, B. E. Saleh, A. V. Sergienko, and M. C. Teich, "Quantum-optical coherence tomography with dispersion cancellation," Phys. Rev. A **65**, 053817 (2002).
20. K. Zielnicki, A. B. U'Ren, and P. Kwiat, "Joint spectral measurement," (2014). Unpublished.
21. C. K. Hong, Z. Y. Ou, and L. Mandel, "Measurement of subpicosecond time intervals between two photons by interference," Phys. Rev. Lett. **59**, 2044–2046 (1987).
22. M. A. Nielsen and I. L. Chuang, *Quantum Computation and Quantum Information (Cambridge Series on Information and the Natural Sciences)* (Cambridge University, 2000).
23. J. H. Eberly, "Schmidt analysis of pure-state entanglement," Laser Phys. **16**, 921–926 (2006).
24. L. E. Vicent, A. B. U'Ren, R. Rangarajan, C. I. Osorio, J. P. Torres, L. Zhang, and I. A. Walmsley, "Design of bright, fiber-coupled and fully factorable photon pair sources," New J. Phys. **12**, 093027 (2010).
25. D. Branning, W. Grice, R. Erdmann, and I. Walmsley, "Engineering the indistinguishability and entanglement of two photons," Phys. Rev. Lett. **83**, 955–958 (1999).
26. P. G. Evans, R. S. Bennink, W. P. Grice, T. S. Humble, and J. Schaake, "Bright source of spectrally uncorrelated polarization-entangled photons with nearly single-mode emission," Phys. Rev. Lett. **105**, 253601 (2010).
27. R. Rangarajan, "Photonic sources and detectors for quantum information protocols: A trilogy in eight parts," Ph.D. thesis, University of Illinois at Urbana-Champaign, United States – Illinois (2010).
28. W. Wasilewski, P. Wasylczyk, P. Kolenderski, K. Banaszek, and C. Radzewicz, "Joint spectrum of photon pairs measured by coincidence fourier spectroscopy," Opt. Lett. **31**, 1130–1132 (2006).
29. M. Avenhaus, A. Eckstein, P. J. Mosley, and C. Silberhorn, "Fiber-assisted single-photon spectrograph," Opt. Lett. **34**, 2873 (2009).
30. A. Christ, K. Laiho, A. Eckstein, K. N. Cassemiro, and C. Silberhorn, "Probing multimode squeezing with correlation functions," New J. Phys. **13**, 033027 (2011).
31. P. G. Kwiat, E. Waks, A. G. White, I. Appelbaum, and P. H. Eberhard, "Ultrabright source of polarization-entangled photons," Phys. Rev. A **60**, R773 (1999).
32. R. Rangarajan, M. Goggin, and P. Kwiat, "Optimizing type-i polarization-entangled photons," Opt. Express **17**, 18920–18933 (2009).
33. J. S. Bell, "On the problem of hidden variables in quantum mechanics," Rev. Mod. Phys. **38**, 447–452 (1966).
34. O. Guhne and G. Toth, "Entanglement detection," Phys. Rep. **474**, 1–75 (2009).
35. J. Schwinger, "Unitary operator bases," Proc. Natl. Acad. Sci. USA **46**, 570 (1960).
36. A. Migdall, "Polarization directions of noncollinear phase-matched optical parametric downconversion output," J. Opt. Soc. Am. B **14**, 1093 (1997).
37. R. Rangarajan, A. B. U'Ren, and P. G. Kwiat, "Polarization dependence on downconversion emission angle: investigation of the 'migdall effect'," J. Mod. Opt. **58**, 312–317 (2011).
38. T. Herzog, J. Rarity, H. Weinfurter, and A. Zeilinger, "Frustrated two-photon creation via interference," Phys. Rev. Lett. **72**, 629–632 (1994).
39. T. Herzog, P. Kwiat, H. Weinfurter, and A. Zeilinger, "Complementarity and the quantum eraser," Phys. Rev. Lett. **75**, 3034–3037 (1995).
40. W. Grice, R. Bennink, P. Evans, T. Humble, and J. Schaake, "Auxiliary entanglement in photon pairs for multi-photon entanglement," J. Mod. Opt. 1–8 (2012).
41. Z. H. Levine, J. Fan, J. Chen, A. Ling, and A. Migdall, "Heralded, pure-state single-photon source based on a potassium titanyl phosphate waveguide," Opt. Express **18**, 3708 (2010).
42. J. Mower and D. Englund, "Efficient generation of single and entangled photons on a silicon photonic integrated chip," Phys. Rev. A **84**, 052326 (2011).
43. J. B. Spring, P. S. Salter, B. J. Metcalf, P. C. Humphreys, M. Moore, N. Thomas-Peter, M. Barbieri, X.-M. Jin,

#228272 - $15.00 USD Received 2 Jan 2015; revised 10 Mar 2015; accepted 10 Mar 2015; published 18 Mar 2015

N. K. Langford, W. S. Kolthammer, M. J. Booth, and I. A. Walmsley, "On-chip low loss heralded source of pure single photons," Opt. Express **21**, 13522 (2013).
44. G. Harder, V. Ansari, B. Brecht, T. Dirmeier, C. Marquardt, and C. Silberhorn, "An optimized photon pair source for quantum circuits," Opt. Express **21**, 13975 (2013).
45. M. D. Eisaman, J. Fan, A. Migdall, and S. V. Polyakov, "Invited review article: Single-photon sources and detectors," Rev. Sci. Instrum. **82**, 071101 (2011).
46. D. Rosenberg, A. J. Kerman, R. J. Molnar, and E. A. Dauler, "High-speed and high-efficiency superconducting nanowire single photon detector array," Opt. Express **21**, 1440 (2013).
47. F. Marsili, V. B. Verma, J. A. Stern, S. Harrington, A. E. Lita, T. Gerrits, I. Vayshenker, B. Baek, M. D. Shaw, R. P. Mirin, and et al., "Detecting single infrared photons with 93% system efficiency," Nature Photon **7**, 210–214 (2013).

1. Introduction

Non-classical light has been exploited for a number of purposes, ranging from testing quantum nonlocality [1,2], to various quantum-enhanced technologies including quantum computation [3–5], quantum teleportation [6,7], and quantum cryptography [8,9]. The nonlinear optical process of spontaneous parametric downconversion (SPDC) is commonly used to generate photon pairs for these applications. The fact that the daughter photons are produced in pairs leads to signal-idler photon-number correlations, so that detection of a single photon in the signal mode heralds, under ideal conditions, the presence of exactly one idler photon at a known position in space and time [10]. This can be generalized, so that the detection of n signal photons can herald the presence of an idler n-photon Fock state [11,12]. Furthermore, as is well known, SPDC sources can be configured to generate photon pairs which are entangled in various discrete degrees of freedom such as polarization [13], time-bin [14], and orbital angular momentum [15]. In this paper we address the question of how to engineer the biphoton quantum state to be factorable in *continuous* degrees of freedom so as to attain two important goals: i) the generation of spectrally-pure heralded single photons, and ii) the generation of photon pairs which are entangled in a discrete photonic variable (polarization in our case), but which are otherwise unentangled.

Unfortunately, SPDC often results in undesired correlations in frequency-time and transverse momentum-position between the two photons in a given pair [16,17], which as is well known leads to heralded single photons which are not in a quantum-mechanically pure state [18]. Such heralded single photons, which are described as a statistical mixture of the allowed spectral and spatial modes, cannot interfere with other single photons, and therefore cannot be used as the basis for scalable quantum information processing. Additionally, polarization-entangled photon pairs can range from factorable to highly-entangled in frequency-time and in transverse position-momentum. The presence of the latter type of entanglement can introduce distinguishing information which can degrade the performance of quantum information schemes employing multiple such sources. Typical sources rely on spectral and spatial filtering in order to achieve the two goals stated in the previous paragraph, at the cost of a significant reduction in source brightness, as well as a reduction of SPDC bandwidth. Here we report on a source geometry which can attain both of these goals, depending on whether we use one or two nonlinear crystals, crucially, without the need for spectral filtering. An added bonus is that since no spectral filtering is used, the photon pairs exhibit a considerably greater bandwidth than typical SPDC sources. This could be important, for example, if used for quantum optical coherence tomography [19]. This engineered source makes use of vector group-velocity matching, and a broadband pump.

In this work we have employed four independent methods to characterize our single-crystal source [20] and to verify that we have attained our two goals stated above: i) mapping the joint spectrum through frequency-to-time conversion in an optical fiber, ii) mapping the joint spectrum using a novel variation of Fourier transform spectroscopy, iii) measuring the (mode-

#228272 - $15.00 USD Received 2 Jan 2015; revised 10 Mar 2015; accepted 10 Mar 2015; published 18 Mar 2015

dependent) $g^{(2)}$ correlations in one arm of the source, and iv) measuring the Hong-Ou-Mandel (HOM) interference between heralded single photons from two independent single-crystal sources [21]. Additionally, in a fifth measurement, we directly verify the presence of polarization entanglement for a two-crystal version of our source.

2. Engineering spectral and spatial unentanglement

The properties of SPDC are defined by conservation of energy and momentum. A narrow pump bandwidth, for example, leads to strict frequency anti-correlation between the signal and idler photons due to conservation of energy. Additionally, correlations due to momentum conservation in the longitudinal direction depend on the crystal length, and in the transverse direction on the degree of pump focusing. Taken together, these constraints define the joint amplitude function; engineering a factorable source depends critically on the crystal and pump parameters.

To describe the spectral correlations present between pairs of photons, we use the joint spectral intensity, a probability distribution in the frequency space of the two-photon state. We are concerned with whether this joint spectrum is *separable* or *correlated*, that is to say, whether it describes a two-photon state that can be written as a separable product state of two single-photon states, or an entangled state which cannot.

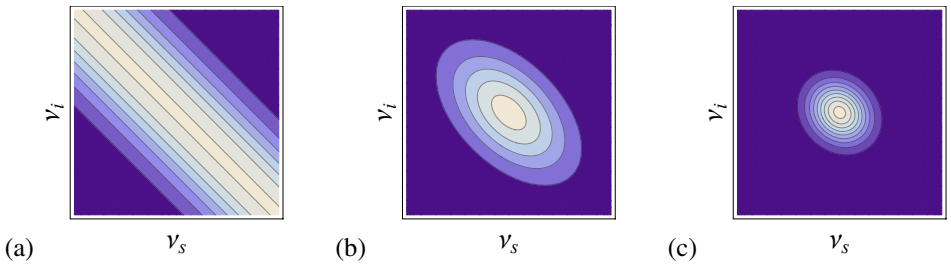

Fig. 1. Simplified model of JSI with frequency correlations due to conservation of energy. Spectral filters reduce correlation; shown in (a) no filtering, (b) filter width equal to the pump bandwidth, and (c) filter width equal to $\frac{1}{5}$ of the pump bandwidth.

We quantify the degree of correlation using the Schmidt decomposition [22, 23], which allows a pure state of a composite system AB to be decomposed into a sum over products of orthonormal states of A and B:

$$f_{A,B} = \sum_i \sqrt{\lambda_i} g_{A,i} g_{B,i}, \tag{1}$$

where the Schmidt coefficients $\sqrt{\lambda_i}$ satisfy the normalization condition $\sum_i \lambda_i = 1$. The Schmidt coefficients can be used to define the Schmidt number K, which can be described as the effective number of populated eigenmodes:

$$K = \frac{1}{\sum_i \lambda_i^2}. \tag{2}$$

The inverse Schmidt number $1/K$ is also equal to the purity P of a heralded single-photon, and the visibility V in a two-source HOM interferometer [24].

2.1. *Spectrally filtered source*

As mentioned in the introduction, an ideal photon pair source for scalable optical quantum information processing should not exhibit spectral or spatial correlations between signal and idler photons. While narrow filters can be used to reduce or even effectively eliminate these

#228272 - $15.00 USD Received 2 Jan 2015; revised 10 Mar 2015; accepted 10 Mar 2015; published 18 Mar 2015

correlations, this solution has a significant downside: if the photons are highly correlated, the required filters are so narrow that they block the majority of the photon pairs available. This can be easily seen from a plot of the joint spectrum in Fig. 1(a): an uncorrelated subset of the joint spectrum will contain only a small fraction of the total photon pair flux (in the theoretical case of a maximally correlated joint spectrum, the fraction is actually zero). Another way to see this is through the Schmidt decomposition: the best filtered, uncorrelated collection mode one can hope for is the most populated Schmidt mode. If the Schmidt number is large, there are many significantly populated Schmidt modes, and any one of them will contain only a small fraction of the total intensity.

Instead of employing spectral filtering to "fix" a highly-correlated source, it would be desirable to produce a joint spectrum which is already *intrinsically* uncorrelated. The following section describes how this can be achieved by manipulating the SPDC phase-matching conditions, using one of the family of "engineered source" techniques [16, 17, 24–26].

2.2. *Factorable joint spectrum*

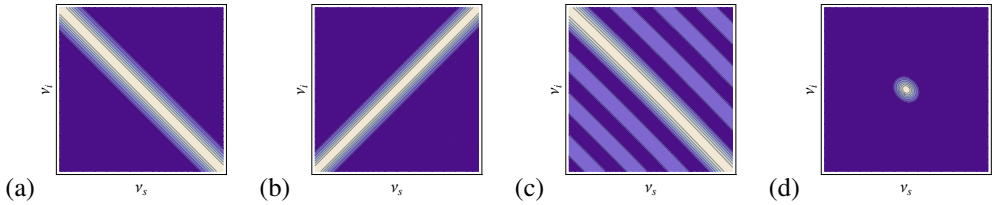

Fig. 2. Joint spectral intensity correlations arising from the various components of the joint spectral intensity, including (a) energy envelope, (b) transverse momentum, (c) longitudinal momentum, and (d) the overall JSI formed by the product of these. This demonstrates how energy and momentum conservation constraints can compensate each other to produce an approximately factorable joint spectrum without spectral filtering. Also note that the longitudinal phase-matching sinc lobes (in c) may be supressed.

The simplified picture presented in Fig. 1 only accounts for conservation of energy between the pump and the SPDC photons, and in particular does not take into consideration phase-matching effects in the crystal. We also considered only the joint spectral *intensity*, whereas correlations can also be present in the joint spectral phase, which is critical for the case of a chirped pump. Finally, we entirely neglected spatial correlations, another important source of non-separability. In practice, spatial correlations are generally eliminated by collecting into single-mode fiber. However, this has the same effect as spectral filtering in reducing source brightness, so ideally we wish to reduce spatial correlations before collection and to carefully choose a collection mode which is highly populated. Moreover, there can be cross-correlations between spatial and spectral modes [24].

To engineer a source of factorable photons, one must calculate the dependence of frequency and spatial correlations on the physical parameters of the SPDC source. The state produced by SPDC can be expressed in terms of creation operators, the signal and idler wavevectors $\vec{k}_s$ and $\vec{k}_i$, and a constant η as

$$|\psi\rangle = |\text{vac}\rangle + \eta \int d\vec{k}_s \int d\vec{k}_i F(\vec{k}_s,\vec{k}_i)\hat{a}_s^\dagger(\vec{k}_s)\hat{a}_i^\dagger(\vec{k}_i)\,|\text{vac}\rangle\,. \tag{3}$$

Here, F is the joint two-photon amplitude (JTPA), which can be written as

$$F(\vec{k}_s,\vec{k}_i) = \ell(\vec{k}_s)\ell(\vec{k}_i)\alpha(\omega_s+\omega_i)\phi(\vec{k}_s,\vec{k}_i), \tag{4}$$

#228272 - $15.00 USD Received 2 Jan 2015; revised 10 Mar 2015; accepted 10 Mar 2015; published 18 Mar 2015

where $\ell(\vec{k}_s)$ and $\ell(\vec{k}_i)$ are separable terms, $\alpha(\omega)$ is the pump spectral amplitude (assumed to be Gaussian), and $\phi(\vec{k}_s,\vec{k}_i)$ is the phase-matching function. In an ideal situation, all the terms in the JTPA would be separable, so that we would be able to write $F(\vec{k}_s,\vec{k}_i) = S(\vec{k}_s)I(\vec{k}_i)$ for specific functions $S(\vec{k}_s)$ and $I(\vec{k}_s)$, each of which depend exclusively on the variables which correspond to one of the two photons. Under these circumstances, no correlations exist between the signal and idler photons, and the source is therefore factorable, with each photon individually in a pure state. Unfortunately, $\alpha(\omega_s+\omega_i)$ and $\phi(\vec{k}_s,\vec{k}_i)$ are *not* in general factorable. However, by adjusting the appropriate parameters of the system, these terms can be made approximately separable. To see how, first consider the full form of the phase-matching function [24],

$$\phi(\vec{k}_s,\vec{k}_i) = \exp\left[-\frac{w_0^2}{4}(k_x^2+k_y^2)\right]\operatorname{sinc}\left[\frac{L}{2}\Delta k\right]\exp\left[i\frac{k_x^2+k_y^2}{2k_p}z_0\right]\exp\left[i\frac{L}{2}(k_p+k_z+k_y\tan\rho_0)\right] \tag{5}$$

$$\Delta k = k_p - k_z - \frac{k_x^2+k_y^2}{2k_p} + k_y\tan\rho_0 \tag{6}$$

where L is the length of the downconversion crystal, $k_p = \left|\vec{k}_p\right|$ is the pump wavenumber, w_0 is the pump beam waist, z_0 is the distance from the pump beam waist to the center of the downconversion crystal, ρ_0 is the spatial walkoff angle, and k_x, k_y, and k_z are the components of the sum of the signal and idler wavevectors, $\vec{k} = \vec{k}_s + \vec{k}_i$.

Table 1. Conditions for SPDC separability [24,27] where k' is the reciprocal group velocity ($\frac{dk}{d\omega}$), w_o and σ are the pump beam waist and bandwidth respectively, L is the crystal length, θ_s and θ_i are the signal and idler emission angles inside the crystal, Φ_{max} is the maximum angular spread about the signal and idler emission angles, and ρ_0 is the walkoff angle. Condition (4) assumes frequency-degenerate collection, while (1) - (3) apply generally.

(1)	$\begin{cases} k'_S = k'_p\cos\theta_s \\ k'_i = k'_p\cos\theta_i \end{cases}$
(2)	$\dfrac{w_o^2}{0.193L^2} = -\tan\theta_s\tan\theta_i$
(3)	$\sigma \gg \dfrac{2}{0.193L(k'_p - k'_s\cos\theta_s)}$
(4)	$\Phi_{max}^2\left(w_0^2 + 0.193\rho_0^2L^2\right) \lesssim \dfrac{1}{k^2\sin^2\theta_0}$

Transforming this into spherical coordinates $\{\omega_s,\theta_s,\phi_s,\omega_i,\theta_i,\phi_i\}$ and Taylor-expanding to first order provides a set of constraints to satisfy in order for non-separable cross terms to vanish, and thus for the source to be factorable [24]. These constraints are detailed in Table 1; they can be described as follows: (1) choosing the collection angles θ_s and θ_i so that the longitudinal component of the signal and idler group velocities match the pump group velocity, (2) selecting the pump beam waist and crystal length according to the collection angles, (3) using a pump bandwidth σ larger than a threshold value which is inversely proportional to crystal length, and (4) collecting photons in a small angular spread around θ_s and θ_i. We refer to condition (1) as vector group velocity matching. The conservation constraints of the pump

#228272 - $15.00 USD Received 2 Jan 2015; revised 10 Mar 2015; accepted 10 Mar 2015; published 18 Mar 2015

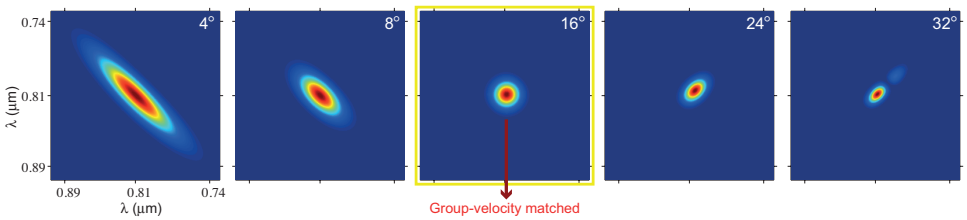

Fig. 3. Predicted dependence of joint spectrum on downconversion emission angle (indicated in the upper right corner of each plot). The optimally separable case occurs when the pump group velocity matches the longitudinal component of the signal and idler group velocities.

envelope and phase-matching function are shown graphically in Fig. 2, demonstrating how a nearly separable joint spectrum can be obtained by appropriate selection of source parameters.

2.3. The engineered source

We have applied these conditions to type-I degenerate SPDC using a β-barium borate (BBO) crystal, pumped with a beam centered at 405-nm, produced by frequency doubling the beam from an ultrafast titanium-sapphire laser (35-fs pulse duration, 76-MHz repetition rate, and centered at 810-nm). The wavelength is chosen based on the availability of ultrafast lasers and efficient single-photon detectors, compared to telecom wavelengths where avalanche photodiode (APD) detector efficiencies are much lower (commercial APD quantum efficiencies for 1550 nm and 810 nm are $\sim 25\%$ and $\sim 60\%$, respectively). The optimal external collection angle is found to be the angle that vector matches the group velocity of the pump and daughter photons ($\theta_{s0} = -\theta_{i0} \approx 16^\circ$ external to the SPDC crystal in our source), as shown in Fig. 3. The additional constraints of Table 1 could be satisfied by choosing a crystal length of $L = 300\ \mu$m and a pump beam waist of $w_0 = 23.15\ \mu$m [27]. Rather than this theoretically optimal waist size, we use a quasi-optimal and more practical pump beam waist of $w_0 = 60\ \mu$m. Due to astigmatism and ellipticity in the pump (i.e., the output of the frequency doubling crystal), the larger beam waist is more symmetric and thus actually leads to a higher purity than attempting a tighter focus where these effects are more pronounced. Note that our signal and idler photons are collected using single-mode fibers; while the fulfilment of the conditions in Table 1 means that our photon pairs are close to factorable in the spatial and spectral degrees of freedom, collection into single-mode fibers eliminates by design any remaining spatial or cross spectral-spatial entanglement. This leaves frequency as the only degree of freedom in which entanglement can reside; we employ broad bandwidth 80-nm FWHM band-pass Semrock filters to exclude scattered pump photons without significantly impacting the SPDC spectrum. For comparison, in some measurements we also employ narrower 20-nm filters to partially filter the joint spectrum. Using a 100-mW pump beam, we observe a detected pair collection rate into single-mode fiber of $\sim 10,000$ pairs per second.

3. Measurement: pure-state heralded single photons

The purity of heralded single photons can be characterized using several methods which either reconstruct the joint spectral intensity or provide a proxy to heralded single-photon purity [20]. Our one-crystal source designed to yield pure-state heralded single photons was discussed in the previous section and is sketched in Fig. 4(a). The four techniques which we have used to characterize this source are shown in Figs. 4(b)-(e), with experimental details explained in the figure caption. These measurement techniques are discussed below, with particular attention to

#228272 - $15.00 USD Received 2 Jan 2015; revised 10 Mar 2015; accepted 10 Mar 2015; published 18 Mar 2015

a novel extension of Fourier transform spectroscopy.

Two-dimensional Fourier transform spectroscopy can be used to measure frequency correlations in the time domain [28]; our experimental implementation is shown in Fig. 4(b). This exploits a self-interference effect and the property that the extremely short (~femtosecond) time regime of the electric field oscillations is easily accessible by an optical delay in a bulk optical medium. Our novel extension of this technique allows us to characterize the joint spectrum with a one-dimensional rather than two-dimensional scan. Under the assumption that the JSI is approximately Gaussian (which is valid for our source), the correlations between the signal and idler are manifested in the diagonal dimensions of the Gaussian ellipse. So, taking the Fourier transform of a 1D scan along the $t_s + t_i$ axis yields the projection of the 2D spectrum along the $f_s + f_i$ axis, as shown in Fig. 5. If we model the joint frequency spectrum as a 2D Gaussian ellipse, the relevant parameter for spectral correlation is the ratio of the peak widths along the $f_s + f_i$ and $f_s - f_i$ axes, σ_d/σ_a. The parameters σ_d and σ_a can be extracted directly from the 1D scan described above, characterizing the Gaussian ellipse

$$f(\nu_s,\nu_i) = A\exp\left[-\left(\nu_s^2+\nu_i^2\right)\left(\frac{1}{4\sigma_d^2}+\frac{1}{4\sigma_a^2}\right) -2\nu_s\nu_i\left(\frac{1}{4\sigma_a^2}-\frac{1}{4\sigma_d^2}\right)\right]. \tag{7}$$

We can determine the heralded single-photon purity P (or equivalently, the inverse Schmidt number $1/K$) directly from a Gaussian ellipse. Applying a change of variables and solving for σ_a and σ_d in terms of σ and σ_f, we can determine the purity as

$$P = \sqrt{1-\left(\frac{r-1}{r+1}\right)^2}, \tag{8}$$

where $r \equiv \sigma_d^2/\sigma_a^2$. Our measurements of the joint spectral intensity implies a purity of 0.88 ± 0.02 without spectral filtering and 0.99 ± 0.01 with 20nm filters, as shown in Fig. 6.

Another promising measurement technique uses dispersion in an optical fiber, which permits the indirect measurement of frequency through the times of arrival [29]; see Fig. 4(c). The experimental setup used is shown in Fig. 4(b). Our fiber (Nufern 780HP) has dispersion of approximately -120 ps/nm per km of fiber, for light near 810 nm. For example, in our 400 m of fiber, a photon with a wavelength of 809 nm will be delayed by approximately 50 ps compared to a photon at 810 nm. Thus, measuring the arrival time of a photon determines its wavelength, assuming that the relative delay exceeds the detector timing jitter. This measurement yields a purity of 0.87 ± 0.03 without spectral filtering, and 0.995 ± 0.04 with 20-nm filters. Our experimental data is shown in Fig. 6(b).

It is important to note that neither of the above measurements account for potential *phase* correlations. These correlations will impact heralded single-photon purity, and can be measured with a two-source Hong-Ou-Mandel interferometer. Conveniently, a measurement of the second-order correlation function in a single SPDC arm also allows us to obtain the number of downconversion modes collected, and thus is an indirect measurement of correlation [30]. The second-order correlation function is straightforward to measure with a Hanbury Brown-Twiss interferometer, as shown in Fig. 4(d). This measurement is also useful for calibration of excess dispersion in the pump, as shown in Fig. 7. A correlation function measurement implies a purity of 0.66 ± 0.02 without filtering and 1.02 ± 0.02 with 20-nm filters.

Finally, the single-photon purity for the spectrally unfiltered case is confirmed through a two-source Hong-Ou-Mandel interferometer [25], shown in Fig. 4(e). In this four-photon measurement, the two sources are two orthogonally-oriented BBO crystals so that in each of the signal

#228272 - $15.00 USD Received 2 Jan 2015; revised 10 Mar 2015; accepted 10 Mar 2015; published 18 Mar 2015

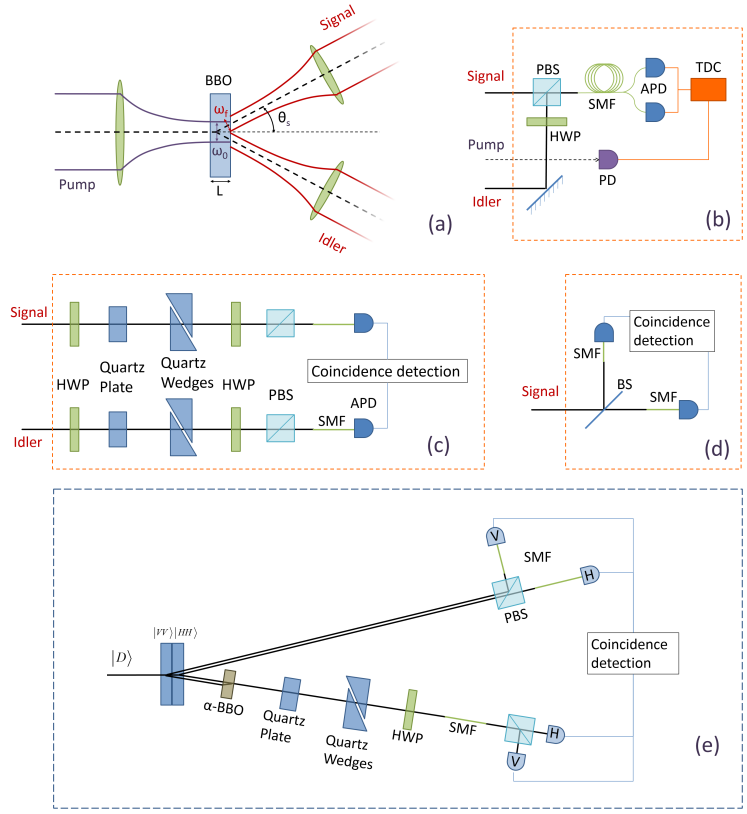

Fig. 4. Schematic diagrams of: (a) Source geometry and relevant parameters in our implementation of the engineered source, used for all following measurements. The pump is focused to a waist of $w_0 = 60\mu$m. The signal and idler collection modes are oriented at $\pm 16^\circ$ with respect the pump axis and are characterized by a beamwaist of 55 μm); these modes meet at the approximate center of the BBO crystal of length $L = 300\mu$m. The signal and idler modes are collimated before passing through additional measurement-dependent optics (e.g., waveplates and polarizers), and finally are collected into single-mode fiber (note that the fiber-coupling optics are not shown). (b) Fiber spectroscopy. A half-wave plate (HWP) and polarizing beamsplitter (PBS) are used to combine the signal and idler modes into a 400-m length of single-mode fiber (SMF). A fiber beamsplitter delivers light to two avalanche photodiodes (APD), which are analyzed by a time-to-digital converter (TDC) together with a synchronization signal from the pump via a photodiode (PD). (c) Two-dimensional Fourier spectroscopy. The common-path polarization interferometer uses a half-wave plate to rotate light into the diagonal basis, followed by a birefringent quartz plate to initially delay horizontally polarized light (H) relative to vertically polarized light (V). Then, quartz wedges are used to variably delay V relative to H. Finally, another HWP rotates back into the H/V basis and a polarizing beam splitter is used to pick off the H component. Two of these polarization interferometers are used in coincidence to analyze the joint spectrum. (d) Correlation function measurement. We measure $g^{(2)}$ in one arm of SPDC using a Hanbury Brown-Twiss interferometer. (e) Two-source Hong-Ou-Mandel interferometer. We herald the presence of one photon pair produced from each of two orthogonally oriented BBO crystals. A suppression of four-fold coincidence counts at zero delay indicates the absence of which-crystal distinguishing information. A relative signal-idler delay can be introduced by a pair of quartz wedges in one arm.

#228272 - $15.00 USD Received 2 Jan 2015; revised 10 Mar 2015; accepted 10 Mar 2015; published 18 Mar 2015

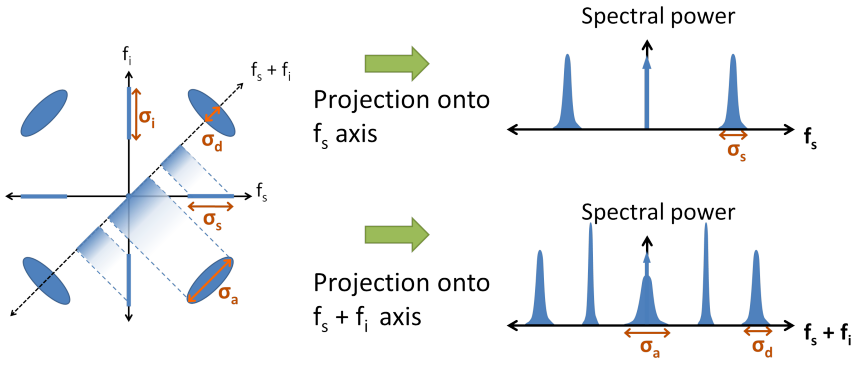

Fig. 5. Sketch of the frequency-domain signal resulting from two-dimensional Fourier spectroscopy.

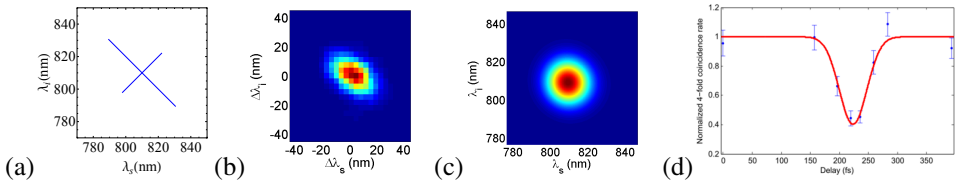

Fig. 6. (a-c) Comparison of measurements of the engineered source joint spectrum with no spectral filtering and an 8-nm bandwidth pump using (a) diagonal Fourier spectroscopy (b) fiber spectroscopy and (c) a theoretical simulation showing ideal behavior. Corresponding purities are (a) 0.88 ± 0.02, (b) 0.87 ± 0.03, and (c) 0.998. (d) Results from two-source HOM with visibility 0.61 ± 0.05. This is in agreement with accompanying $g^{(2)}$ measurements, which imply a maximum visibility of 0.66 ± 0.02. The line shown is a Gaussian fit to the data.

and idler arms there is one horizontally-polarized and one vertically-polarized photon. We prepare two photons in the idler arm, which are to be interfered with each other, by triggering on the detection of two corresponding photons in the idler arm. The two heralded photons in the signal arm are temporally and spatially compensated, their polarizations are rotated from horizontal-vertical to diagonal-antidiagonal using a halfwave plate before passing through a polarizing beamsplitter in the H/V basis. A delay between the two idler photons can be introduced by a pair of quartz wedges. In contrast to a typical Hong-Ou-Mandel measurement where interference takes place between two spatial modes of a beamsplitter, here interference takes place between two polarizations sharing the same (idler-photon) spatial mode. We observe a visibility (or single-photon purity) of 0.61 ± 0.05, shown in Fig. 6(d).

4. Measurement: polarization entanglement

An important advantage of this engineered source is the relative ease of employing it as a source of polarization-entangled photons using a standard two-crystal geometry [31], as shown in Fig. 8. This method uses two identical but orthogonally oriented type-I SPDC crystals, such that the first converts horizontally (H) polarized pump photons to pairs of vertically (V) polarized photons, while the second takes V pump photons to H pairs. Thus, a diagonally polarized pump ideally produces a maximally entangled polarization state. Note that the spatio-temporal engineering discussed above in the context of the single-crystal source applies separately to each of

#228272 - $15.00 USD Received 2 Jan 2015; revised 10 Mar 2015; accepted 10 Mar 2015; published 18 Mar 2015

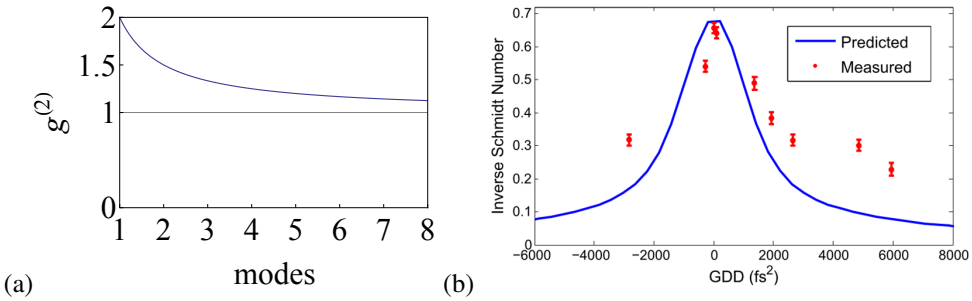

Fig. 7. (a) Calculated relationship between $g^{(2)}$ for a source with K (effective) thermal modes. (b) Measured values of inverse Schmidt number $1/K$, measured from the correlation function. This is equal to heralded single-photon purity or $g^{(2)}(0)$ - 1. The horizontal axis shows a variable amount of group delay dispersion (GDD) applied to our pump using a prism-pair compressor, controlling pump temporal chirp. A simple prediction based only on second- and third-order dispersion is shown in blue.

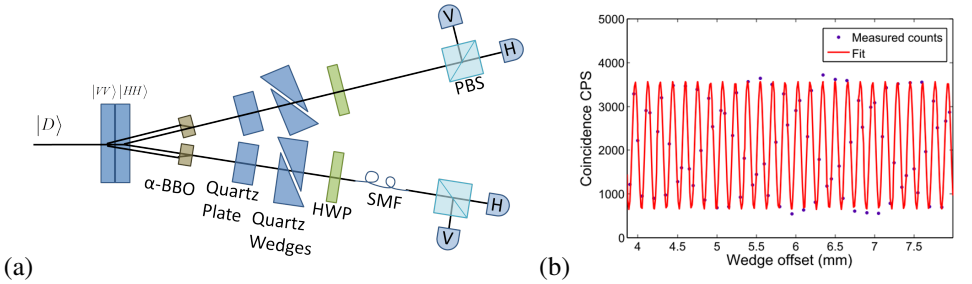

Fig. 8. (a) Diagram of the two-crystal scheme for polarization entanglement. We use a diagonally polarized pump and two orthogonally oriented type-I SPDC crystals to produce pairs of polarization-entangled photons. The crystal labels indicate the polarization of the SPDC cone produced by each crystal. Due to the spatial separation of the two crystals, we use walk-off in birefringent α-BBO to combine the photons into a single spatial mode. The quartz plate and quartz wedges compensate for the temporal delay between the photons. (b) Diagonal-diagonal coincidence counts as a function of phase offset between H and V, demonstrating polarization correlation / anticorrelation.

the two crystals used in the two-crystal source. Indeed, all of the parameters of each of the two crystals in the two-crystal source are identical to the parameters of the single-crystal source.

To produce a polarization-entangled state rather than a mixed state, there must be no way to determine which crystal a particular photon was produced in. Distinguishing information may be present spectrally, spatially, or temporally. Spectral distinguishability is taken care of almost by default, as the two crystals are identical up to a 90° rotation and the spectral distribution of SPDC is rotationally symmetric about the pump.

Spatially, our SPDC crystals have a center-to-center offset of 300 μm, which leads to a 300 $\mu\text{m} \times \sin 16^\circ = 82.69\mu\text{m}$ lateral separation of the desired collection modes. Unless compensated for, this separation makes it impossible to efficiently collect from both crystals. Fortunately, the two crystals produce orthogonal polarizations, so a birefringent compensation crystal can be chosen such that extraordinarily polarized photons will experience precisely enough walk-off to be displaced onto the ordinarily polarized mode, thus "stitching" together the two modes (see Fig. 8). In our source, this compensation can be achieved with a 0.952 mm thick-

#228272 - $15.00 USD Received 2 Jan 2015; revised 10 Mar 2015; accepted 10 Mar 2015; published 18 Mar 2015

ness of α-BBO, cut with the optic axis at 45° to the front surface. In practice, we use 1 mm of α-BBO and adjust the angle of the crystal slightly with respect to the incident light to fine-tune the displacement.

Temporal distinguishability arises from geometrical and birefringent collection time differences between H and V photons, and is especially important given the femtosecond-scale coherence times of our source [32]. For temporal compensation, we use a quartz plate and a pair of quartz wedges in the style of a Soleil-Babinet compensator. Here again we rely on birefringence, but rather than transverse walk-off, the critical property is the optical path length difference (and thus time delay) between ordinary and extraordinary polarization. This time delay is optimized by measuring interferometric visibility as a function of quartz thickness, and in our system can be set within a range of approximately $\pm$300 fs as needed to compensate time-of-arrival differences between the crystals. For our system, an additional time delay of approximately 50 fs is used to compensate the temporal walkoff introduced by the spatial-mode stitching α-BBO crystals.

There are many approaches to detecting and quantifying entanglement, including Bell inequality violation, quantum state tomography, and a variety of entanglement witnesses [33,34]. In our case, we demonstrate that we have produced *polarization* entanglement by observing correlation/anticorrelation in two mutually unbiased bases [35]. We observe visibilities of approximately 0.85 in the H/V basis and 0.75 in the D/A basis. Thus, the sum of mutually unbiased bases exceeds the classical threshold of 1 and clearly demonstrates entanglement, but falls short of the maximum of 2 for a maximally entangled state. The reduction in visibility indicates that there remains some which-crystal distinguishing information, and the quality of entanglement could be improved by more careful calibration and alignment. However, visibility is also limited (to at most 96%) by asymmetric polarization in type-I SPDC. This "Migdall effect" arises because the daughter photons are ordinarily polarized, but ordinary polarization is defined as perpendicular to both the optic axis of the crystal and the direction of propagation of the photon, leading to a dependence on the azimuthal emission angle [36]. Unfortunately for the engineered source, this effect is especially dramatic for large cone angles, and reaches a 12° deviation from vertical polarization for our 16° SPDC cone opening half-angle, resulting in a 4% reduction in fidelity with the maximally entangled state [37].

There are other methods for achieving entanglement in a discrete photonic variable. For example, path entanglement has been demonstrated using the "rail-cross" scheme, in which pumping one SPDC crystal from both sides creates two coherently superposed downconversion paths [38, 39]. Two-photon and multi-photon entangled states have also been implemented by pumping an SPDC crystal in two lateral locations, then recombining downconversion paths according to polarization [40]. These non-polarization-based qubits would enable one to achieve an even higher level of qubit entanglement than the polarization qubits of our current two-crystal approach, while maintaining the spectral non-entanglement.

5. Heralding efficiency

Although, as discussed above, there are compelling reasons to optimize a source so as to obtain a factorable joint spectrum, it is worth noting that a filtered, correlated (i.e. unengineered) source can be more desirable in some cases. For example, it is possible to take advantage of correlations to *improve* heralding efficiency (the probability of detecting an idler photon conditioned on the detection of a signal photon, given by the coincidence detection rate divided by the heralding single-channel detection rate). In the case where *one-way* heralding efficiency is the critical parameter, we can improve heralding efficiency in the desired collection mode by asymmetrically filtering only the complementary mode. It turns out that the unengineered source achieves a higher heralding efficiency under both symmetric and asymmetric spectral

#228272 - $15.00 USD Received 2 Jan 2015; revised 10 Mar 2015; accepted 10 Mar 2015; published 18 Mar 2015

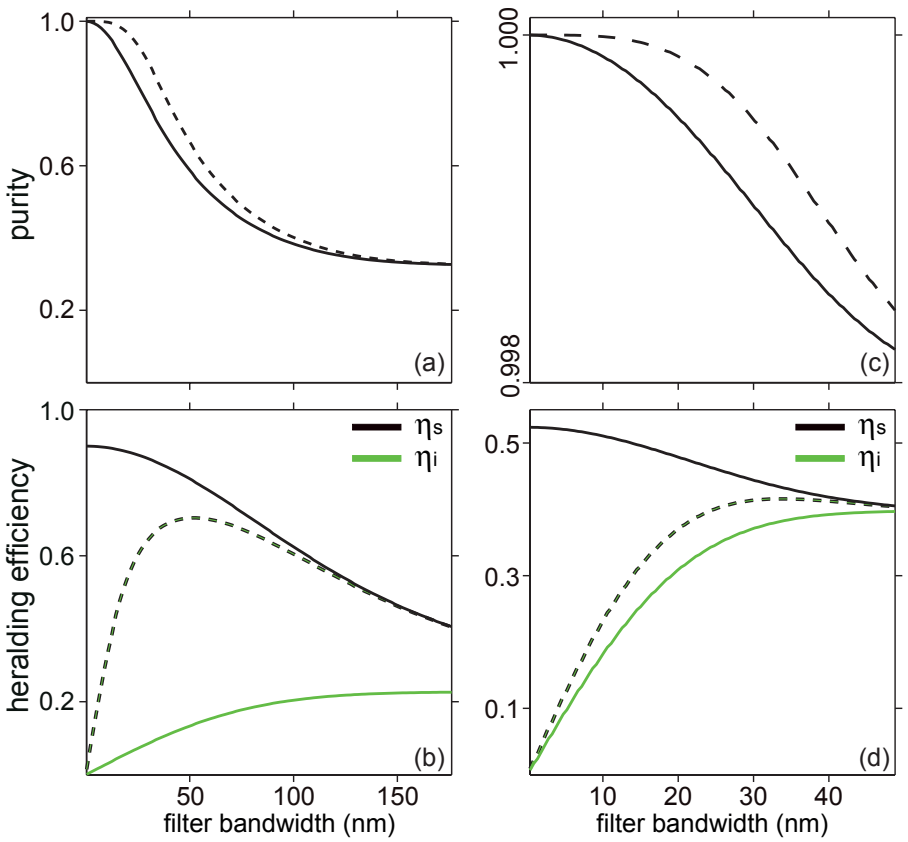

Fig. 9. Calculated purity and heralding efficiency as a function of filter bandwidth with rectangular filters for both (a,b) correlated, unengineered source and (c,d) engineered source. The solid lines show asymmetric collection into the signal and idler modes with filtering applied only to the signal (heralding) photon, shown as solid black line, and applied only to the idler (heralded) photon, shown as solid green line. The dashed lines show symmetric collection with filtering applied to both modes.

filtering, at the cost of a lower heralded single-photon purity when compared to the engineered source.

Results of theoretical calculations of heralding efficiency and heralded single-photon purity, for the correlated and engineered source are shown in Fig. 9. In the figure we show plots of the heralding efficiency and of the single photon purity vs filter bandwidth. The simulations which form the basis for these plots were carried out relying on the theory in Ref. [24]. We have considered three different filtering schemes, involving filtering applied: i) to the *heralded* photon (shown as green solid curves, labeled as η_i), ii) to the *heralding* photon (shown as black solid curves, labeled as η_s), and iii) symmetrically to both photons (shown as dashed curves). Note that both asymmetric filtering schemes lead to the same purity vs filter bandwidth curve, with values lower than those attained for symmetric filtering. In regard to the heralding efficiency, asymmetric filtering of the *heralding* photon yields the best result, while in contrast, asymmetric filtering of the *heralded* photon leads to a significantly poorer performance.

#228272 - $15.00 USD Received 2 Jan 2015; revised 10 Mar 2015; accepted 10 Mar 2015; published 18 Mar 2015

6. Conclusions

Relying on a broadband pump and on vector group velocity matching in the SPDC process, we have been able to attain the two important goals of generating: i) pure heralded single photons, and ii) polarization-entangled photon pairs which are unentangled in all other degrees of freedom. Because our source produces these two types of quantum state intrinsically, in particular without the need for spectral filtering, the bandwidth of our source exceeds 20 nm. We point out that SPDC-based photon pair sources not engineered for factorability typically use filters narrower than 1 nm to achieve the same level of purity.

However, we have found that a trade-off exists between heralding efficiency and single-photon purity. An unengineered source which exhibits strong signal-idler correlations can in fact lead to a higher heralding efficiency as compared to our engineered source. Our source, optimized for single-photon purity, has a heralding efficiency limited to about 40% (after subtracting the effect of a non-ideal detector quantum efficiency). This could limit the usefulness of our source in applications where heralding efficiency is crucial, such as for on-demand single-photon sources. In addition, SPDC waveguide sources [41–44] and telecom-wavelength sources [26] have shown promising results, achieving higher count rates for a similar purity, with a higher heralding efficiency. These approaches appear promising for optical quantum information applications, particularly with the increasing availability of efficient telecom-wavelength detectors [45–47].

Nevertheless, our technique should prove useful in situations where optimized photon pairs are required in the near-IR and/or in situations where polarization entanglement is required in addition to an engineered spatio-temporal character.

Acknowledgments

Funding for this work has been provided in part by NSF Grant No. PHY 09-03865 ARRA, by Office of Naval Research (ONR) Grant No. N00014-13-1-0627, by US Army ARO DURIP Grant No. W911NF-12-1-0562, by CONACYT, Mexico, by DGAPA (UNAM) grant 105915 and by AFOSR grant FA9550-13-1-0071.

#228272 - $15.00 USD Received 2 Jan 2015; revised 10 Mar 2015; accepted 10 Mar 2015; published 18 Mar 2015